5550–5559 *Nucleic Acids Research, 2015, Vol. 43, No. 11* *Published online 04 May 2015*
doi: 10.1093/nar/gkv444

Structural insights into catalysis and dimerization enhanced exonuclease activity of RNase J

Ye Zhao[1,*,†], Meihua Lu[1,†], Hui Zhang[1,2,†], Jing Hu[1], Congli Zhou[1], Qiang Xu[3], Amir Miraj Ul Hussain Shah[1], Hong Xu[1], Liangyan Wang[1] and Yuejin Hua[1,*]

[1]Key Laboratory of Chinese Ministry of Agriculture for Nuclear-Agricultural Sciences, Institute of Nuclear-Agricultural Sciences, Zhejiang University, China, [2]China Tobacco Gene Research Center, Zhengzhou Tobacco Research Institute of CNTC, Zhengzhou, China and [3]Zhejiang Provincial Key laboratory of Radiation Oncology, Zhejiang Cancer Research Institute, Zhejiang Cancer Hospital, Hangzhou, China

Received February 08, 2015; Revised April 24, 2015; Accepted April 24, 2015

ABSTRACT

RNase J is a conserved ribonuclease that belongs to the β-CASP family of nucleases. It possesses both endo- and exo-ribonuclease activities, which play a key role in pre-rRNA maturation and mRNA decay. Here we report high-resolution crystal structures of *Deinococcus radiodurans* RNase J complexed with RNA or uridine 5′-monophosphate in the presence of manganese ions. Biochemical and structural studies revealed that RNase J uses zinc ions for two-metal-ion catalysis. One residue conserved among RNase J orthologues (motif B) forms specific electrostatic interactions with the scissile phosphate of the RNA that is critical for the catalysis and product stabilization. The additional manganese ion, which is coordinated by conserved residues at the dimer interface, is critical for RNase J dimerization and exonuclease activity. The structures may also shed light on the mechanism of RNase J exo- and endonucleolytic activity switch.

INTRODUCTION

The RNA degradosome is a multi-enzyme complex involved in ribosomal RNA processing and messenger RNA degradation (1–4). In Gram-negative bacteria such as *Escherichia coli*, the degradosome is comprised of three major components including endoribonuclease RNase E, RNA helicase RhlB and phosphorolytic exoribonuclease PNPase. RNase E has a central role among these components, as its C-terminal portion is the scaffold for the assembly of the degradosome (5). It is believed that the RNase E cleavage is the rate-limiting step in mRNA degradation (6). However, the RNA degradosome from Gram-positive bacteria, which lack homologs of RNase E, are markedly different. Over the past decade, growing evidence suggests that RNase J plays a crucial role in RNA degradation in Gram-positive bacteria (7–14).

RNase J was the first ribonuclease identified in bacteria which has both endonuclease and 5′-to-3′ exonuclease activity (12,15). It has been thoroughly studied in *Bacillus subtilis*, a Gram-positive bacterium lacking RNase E (10,13,16–18). Two RNase J paralogs were identified in *B. subtilis* that have been named RNase J1 and RNase J2 (12). It was later confirmed that RNase J1 interacts directly with RNase J2 to form an RNase J1/J2 heterotetramer in solution (16). Unlike RNase J1 or the RNase J1/J2 complex that both exhibit strong 5′-to-3′ exonuclease activity, RNase J2 alone has only weak exonuclease activity that is over a hundreds-fold lower (16). It has been shown that the 5′ exonuclease activity of RNase J1 is strongly inhibited when the substrate RNA contains a 5′-triphosphate moiety (10). On the other hand, RNase J1 could digest RNA with 5′-monophosphate or 5′-OH end more efficiently, suggesting that the cleavage of the P-O bonds by RNase J1 generates 5′-phosphate and 3′-OH products (10).

Crystal structures of RNase J orthologues from *Thermus thermophilus* and *B. subtilis* complexed with uridine 5′-monophosphate (UMP) or RNA have recently been determined (19–21). RNase J adopts a modular domain arrangement as a typical β-CASP family nuclease, which comprises a β-lactamase core domain, a β-CASP domain and an extended C-terminal domain. Superimpositions of these structures revealed both open and closed conformations depending on the substrate RNA binding (20), which cause the significant movement between the β-lactamase core domain and β-CASP domain. Protein–RNA interactions are mediated predominantly via electrostatic interactions between the RNA sugar-phosphate backbone and positively charged amino acids, which is consistent with its nonspecific exonuclease activity (20). It is worth notice

*To whom correspondence should be addressed. Tel: +86 571 86971279; Fax: +86 571 86971703; Email: yezhao@zju.edu.cn
Correspondence may also be addressed to Yuejin Hua. Tel: +86 571 86971703; Email: yjhua@zju.edu.cn
†These authors contributed equally to the paper as first authors.

that the active site is essentially identical in both conformations, with two catalytic zinc ions present independent of substrate binding (19,20). Moreover, the structures reveal a strong phosphate-binding pocket located at one nucleotide distance beyond the catalytic center (20,21). The 5′-monophosphate is bound snugly in the pocket, which explains the strong 5′ end preference of RNase J exonuclease activity (20,21). However, the RNA does not sit down properly in the active site, probably due to the absence of one of the catalytic metal ions (20).

We report here the high-resolution crystal structures of wild type *Deinococcus radiodurans* RNase J (Dra-RNase J) complexed with UMP and its catalytically inactive mutant complexed with 6 nt RNA in a functional form. The structures suggest that Dra-RNase J uses two-metal-ion catalysis. A hydroxide ion bridges two catalytic metal ions, which mimic the nucleophilic attack on the substrate RNA. One highly conserved residue interacts with the scissile phosphate of the RNA, which is involved in catalysis and product protonation. Furthermore, divalent cations were found to be important for Dra-RNase J dimerization and enzymatic activity.

MATERIALS AND METHODS

Cloning and expression

Full-length (residues 1–559) and truncated (residues 1–450) Dra-RNase J were amplified by polymerase chain reaction (PCR) and cloned to the modified pET28a expression vector, which contains a fused N-terminal 6×His-tag, a MBP-tag and a TEV protease recognition sequence (His-MBP-TEV) as described (22). Transformed *Escherichia coli* Rosetta (DE3) clones were grown at 37°C in LB medium containing 50 μg ml^{-1} Kanamycin to an optical density at 600 nm of 0.6–0.8. Protein expression was induced at 30°C for 5 h by adding isopropyl-β-D-thioga-lactopyranoside (IPTG) with a final concentration of 0.4 mM. Cells were harvested by centrifugation at 5000 × g for 30 min at 4°C and stored at −80°C. Site directed mutagenesis was performed with a QuikChangeTM Site-Directed Mutagenesis Kit from Stratagene (La Jolla, CA, USA). Primers used for cloning and mutagenesis are listed in Supplementary Table S1.

Protein purification

All the Dra-RNase J proteins (encoded by *D. radiodurans* gene DR2417) were purified in a similar way. Cells resuspended in lysis buffer (20 mM Tris (pH 8.0), 500 mM NaCl, 10% (w/v) glycerol, 3 mM β-ME, 20 mM imidozole) were lysed by sonication and the lysate clarified by centrifugation at 35 000 × g for 30 min at 4°C. The supernatant was purified by HisTrap HP column (GE Healthcare) equilibrated with buffer A (20 mM Tris (pH 8.0), 1 M NaCl, 5% (w/v) glycerol, 3 mM β-ME, 20 mM imidozole), washed with 40 mM imidazole and finally eluted with 300 mM imidazole. After TEV-tag-removal using TEV protease, the protein was loaded onto the MBPTrap HP column (GE Healthcare) to remove the uncleaved protein. The flow-through fractions were collected and loaded onto a HiTrap Q HP column (GE Healthcare) pre-equilibrated with buffer B (20 mM Tris (pH 8.0), 20 mM NaCl, 3 mM DTT, 5% (w/v) glycerol). Fractions containing Dra-RNase J were elute with a linear gradient from 20 mM to 300 mM NaCl and stored at −80°C. To prepare fresh protein for crystallization and biochemical assays, the protein was finally purified by Superdex 200 10/300 GL column (GE Healthcare) with buffer C (20 mM Tris/HCl (pH 8.0), 100 mM KCl, 0.5 mM EDTA).

Crystallization and structure determination

Crystallization trials were carried out by the sitting drop vapor diffusion method at 293 K. Binary complex was prepared by mixing D175A mutant Dra-RNase J and 6 nt RNA (pUUUUUU), which bearing a 5′-monophosphate moiety, at a 1:1.5 molar ratio. The final protein concentration was 4–5 mg/ml. Crystals were grown in 0.1 M MES monohydrate (pH 6.5), 6%-10% (w/v) polyethylene glycol (PEG) 4000 and 0.1 M Mn^{2+} after multiple rounds of optimization. The Dra-RNase J-UMP crystals were grown in the similar condition except the addition of 5 mM UMP instead of RNA. Cryocooling was achieved by stepwise soaking the crystals in reservoir solution containing 10, 20 and 30% (v/v) glycerol for 3 min and flash freezing in liquid nitrogen. Diffraction intensities were recorded on beamline BL17U at Shanghai Synchrotron Radiation Facility (Shanghai, China) and were integrated and scaled with the XDS suite (23). The structures of Dra-RNase J-RNA and Dra-RNase J-UMP were determined by molecular replacement using Tth-RNase J (3T3N) as the search model (24). Structures were refined using PHENIX (25) and interspersed with manual model building using COOT (26). The statistics for data collection and refinement are listed in Table 1. Dra-RNase J forms a dimer in the crystallographic asymmetric unit and the refined structures include 1090 aa of Dra-RNase J (residues 15–559 from each protomer), four catalytic zinc ions, two manganese ions and RNA (RNaseJ-RNA complex) or UMP (Dra-RNase J-UMP complex). All the residues are in the most favorable (98.4%) and allowed regions (1.6%) of the Ramachandran plot. Both structures show poorly defined loop regions for residues 485–492, 522–528 and 556–559. All structural figures were rendered in PyMOL (www.pymol.org).

Nuclease activity assay

All the oligo RNA and DNA were purchased from Sangon (Shanghai) with either 3′- or 5′-end labeled by 6-carboxfluorescein (6-FAM). For a typical nuclease digestion assay, 500 nM RNA was incubated with various concentrations (100–500 nM) of freshly prepared full-length, truncated (1–450) Dra-RNase J or other mutant proteins in a 10 μl reaction volume containing 50 mM Tris (pH 8.0), 100 mM KCl, 0.1 mg/ml BSA, 1 mM DTT and 5 mM $MnCl_2$ at 30°C for 10–30 min. The reactions were stopped with 6×stop buffer (10 mM EDTA, 98% formamide) and incubating at 95°C for 10 min. Reaction products were resolved on 15% polyacrylamide sequencing gels containing 7 M urea. To determine the metal usage, various kinds of metals including $MgCl_2$ (5 mM), $CaCl_2$ (5 mM), EDTA (10 mM) or 1,10-phenanthroline (10 mM) were added in the reaction buffer.

Table 1. Statistics from crystallographic analysis

	RNase J-UMP	RNase J_d-RNA
Data collection		
Space group	P $2_12_12_1$	P $2_12_12_1$
Cell dimensions		
a, b, c (Å)	66.59, 87.76, 253.42	67.10, 87.85, 249.27
α, β, γ (°)	90, 90, 90	90, 90, 90
Wavelength (Å)	1.0000	0.9792
Resolution (Å)	30–2.0 (2.06–2.0)	30–1.7 (1.74–1.70)
R-meas	6.5 (65.7)	10.2 (69.7)
I/σI	16.1 (3.2)	10.7 (1.9)
Completeness (%)	97.5 (98.1)	97.2 (79.8)
Redundancy	6.0	5.9
Refinement		
Resolution (Å)	30–2.0	30–1.7
No. reflections	98253	158299
R_{work}/R_{free}	20.02/23.52	19.49/21.70
No. atoms		
Protein/RNA	8364/-	8347/242
Ligand/Ion	54/6	12/6
Waters	324	760
B factors		
Protein/RNA	55.6/-	39.1/46.5
Ligand/Ion	137.9/42.1	36.2/33.1
Water	50.7	41.7
Rmsd		
Bond length (Å)	0.008	0.007
Bond Angle (°)	1.125	1.139
Ramachandran statistics		
Favored (%)	98.4	98.4
Allowed (%)	1.6	1.6
Outliers (%)	0	0

Values in parentheses refer to the highest resolution shell.
R factor = $\Sigma||F(obs)- F(calc)||/\Sigma|F(obs)|$.
R_{free} = R factor calculated using 5.0% of the reflection data randomly chosen and omitted from the start of refinement.
RNase J_d denotes catalytic inactive Dra-RNase J (D175A)

Phenotypic assay

D. radiodurans R1 ATCC13939 and its derivatives were grown at 30°C either in TGY broth (0.5% tryptone, 0.1% glucose, 0.3% yeast extract) or on TGY agar plate (1.25% agar). Heterozygous C-terminal truncated *D. radiodurans rnaseJ* mutant strain (*rnaseJ* Δ*C*) was constructed by tripartite ligation method as described previously (27). Briefly, the DNA fragments upstream and downstream of C-terminal region of *rnaseJ* were amplified by PCR using the primers: RnjC_upF (5′-AG TCGGCTGACCTGCCCGCTCCCAC); RnjC_upR (5′-TCGGATCCCGCCGCCACGGTGCCCGACACCCG GAAC); RnjC_downF (5′-CGCGAAGCTTGAGGGCAT TTGACAAAAGAATGGCCCTGC); and RnjC_downR (5′-AGCACCTCGCTCAAGTCCGACACCC), respectively. After digestion with *Bam*H1 or *Hind*III, these two fragments were ligated to a predigested kanamycin resistance gene and transformed into *D. radiodurans* R1. The mutant colonies were selected on TGY plates containing 25 μg ml^{-1} kanamycin. Due to the small size of C-terminal depletion, additional primers RnjC_VF (5′-AGAACGGCGACATCGTCAACCTCGG) and RnjC_VR (5′-CTCCGAGTCTCCCCTTGCTTGGTAG) were synthesized to confirm the mutant strain. The growth curves were measured as described previously (27).

RESULTS AND DISCUSSION

The exoribonuclease activity of Dra-RNase J

Dra-RNase J is a 559-amino acids protein conserved within the Deinococcus-Thermus phylum, which shares 56% amino acid identity with the *T. thermophilus* RNase J (Supplementary Figure S1). Sequence alignment showed that Dra-RNase J contains all seven signature motifs of the RNase J family protein, which belongs to β-lactamase core domain (motif I-IV) and β-CASP domain (motif A-C), respectively (Figure 1A and Supplementary Figure S1). To investigate the nuclease activity, Dra-RNase J was incubated with a synthetic 20 nt RNA fluorescent-labeled at either the 3′- or 5′-end in the presence of magnesium ions. The 5′-labeled RNA was quickly digested, which resulted in the rapid accumulation of band that corresponded to the single ribonucleotide (Supplementary Figure S2). In contrast, digestion of 3′-labeled RNA resulted in multiple intermediate bands that corresponded to the cleavage products longer than 1 nt (Supplementary Figure S2). These results indicate that Dra-RNase J, like other RNase J nucleases, performs exonucleolytic degradation in the 5′-to-3′ direction.

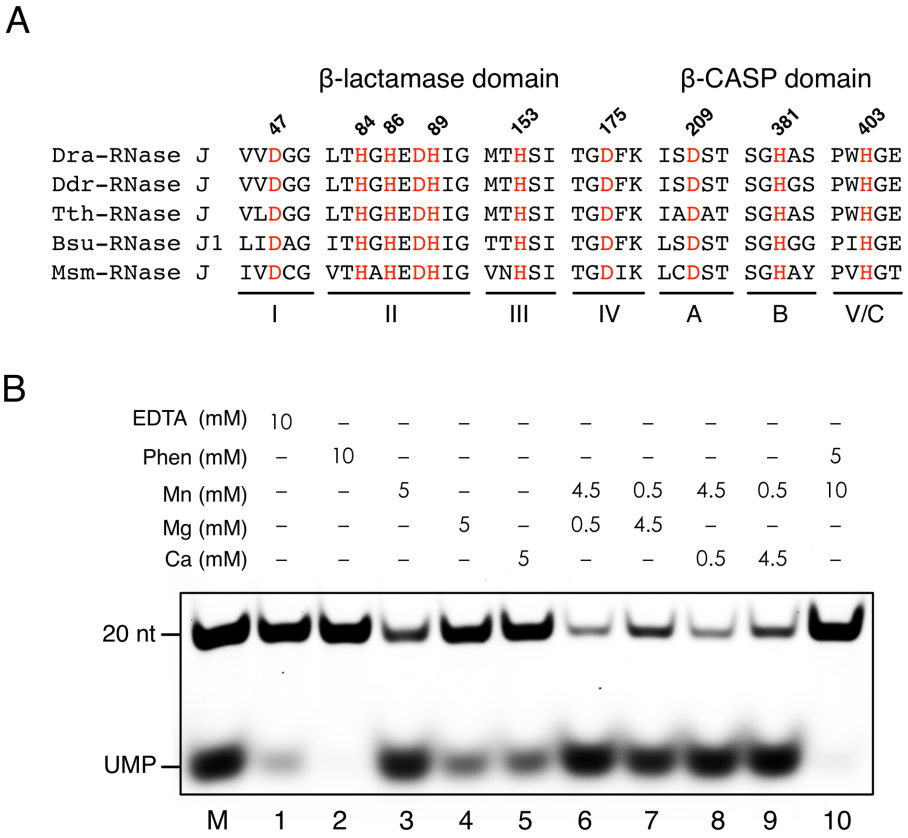

Figure 1. Dra-RNase J is a zinc-dependent β-CASP nuclease with the β-lactamase domain. (**A**) Sequence alignment shows seven signature motifs (highlighted in red) of bacterial RNase J proteins: Dra (*Deinococcus radiodurans*), Ddr (*Deinococcus deserti*), Tth (*Thermus thermophilus*), Bsu (*Bacillus subtilis*) and Msm (*Mycobacterium smegmatis*). Motif I-IV belong to the β-lactamase domain and motif A-C belong to β-CASP domain. (**B**) 5′-fluorescent labeled 20 nt single strand RNA was incubated with Dra-RNase J in the presence of EDTA (lane 1), 1,10-phenanthroline (Phen, lane 2) and various divalent cations (lanes 3–10). For the lane 10, the reaction mixture was pre-incubated with 5 mM 1,10-phenanthroline before adding Mn^{2+} ions.

To further determine the metal preference, various metals including magnesium, calcium or manganese ions were tested (Figure 1B). Purified Dra-RNase J itself showed weak nuclease activity without additional metal ions (data not shown). Similar to other β-CASP family proteins such as CPSF-73 and CPSF-100 (28), high concentrations of EDTA (10 mM) could not totally abolish the Dra-RNase J nuclease activity, while the digestion was strongly inhibited by the addition of 10 mM 1,10-phenanthroline, a high-affinity zinc chelator (Figure 1B, lanes 1 and 2). Incubation with a large excess of manganese ions could only partially restore the nuclease activity when Dra-RNase J was pre-incubated with 1,10-phenanthroline (Figure 1B, lane 10), suggesting that the zinc ions are used for Dra-RNase J catalysis. The exonuclease activity of Dra-RNase J was dramatically stimulated by all the divalent cations tested, but manganese gave the highest activity (Figure 1B, lanes 3–5). Moreover, Dra-RNase J activity in a reaction buffer containing 0.5 mM Mn^{2+} and 4.5 mM of another divalent cation (Mg^{2+} or Ca^{2+}) was almost equal to that with 5 mM Mn^{2+} (Figure 1B, lanes 6–9), further indicating the strong preference for Mn^{2+} ions. Thus, Dra-RNase J is a canonical member of the β-CASP family protein that uses the Zn^{2+} ions for catalysis. Divalent cations, such as Mg^{2+} and Mn^{2+}, could stimulate its nuclease activity *in vitro*.

Overall structure and active site

To investigate the mechanism of catalysis, we determined the crystal structures of Dra-RNase J complexed with UMP (RNaseJ-UMP) and its catalytically inactive mutant complexed with 6 nt RNA (RNaseJ-RNA; Table 1). Crystals were grown in the presence of Mn^{2+} ions and diffracted X-rays to 2.0 and 1.7 Å resolution, respectively. Dra-RNase J crystallizes in space group $P2_12_12_1$, with a dimer molecule in the crystallographic asymmetric unit. Both RNaseJ-UMP and RNaseJ-RNA structures were determined by molecular replacement using Tth-RNase J (PDB code: 3T3N) as the search model. After refinement, these two complexes are superimposable with a root mean square deviation (rmsd) of 0.223 Å over 498 pairs of Cα atoms. The structures are validated by the appearance of well-formed active site that two catalytic metal ions and 6 nt RNA or UMP are observed in the active site (Figure 2A and Supplementary Figure S3). An additional manganese ion is present at the dimer interface in both Dra-RNase J protomers in the crystallographic asymmetric unit (Figure 2A).

Dra-RNase J, which is comprised of 15 α-helices and 25 β-strands (Supplementary Figure S1), contains three domains including an N-terminal β-lactamase domain (residues 5–217 and residues 380–477), an inserted β-CASP domain (residues 218–379) and an extended C-terminal do-

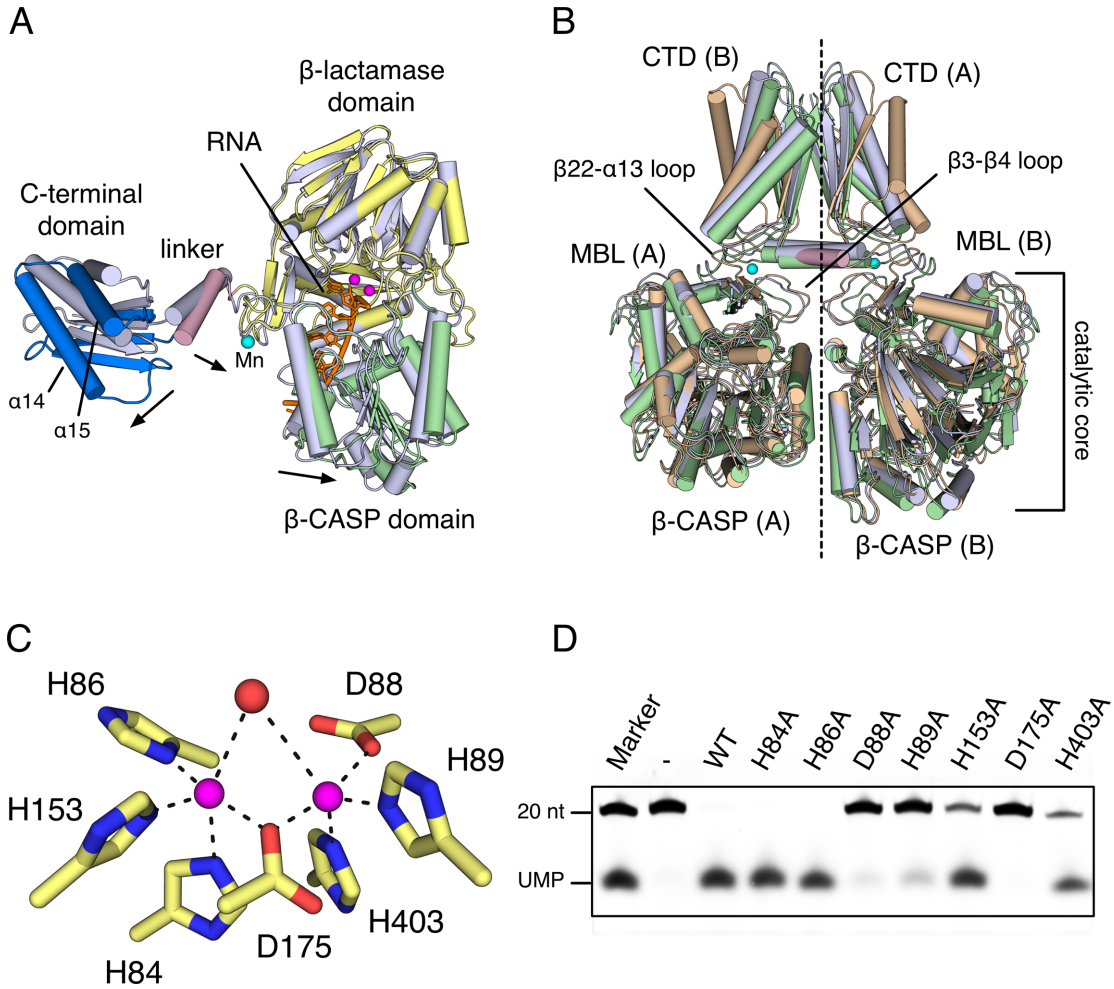

Figure 2. Overall structure and active site. (**A**) Comparison of RNaseJ-RNA and Tth-RNase J/RNA structures. The Tth-RNase J from Tth-RNase J/RNA complex (PDB code: 3T3N) is colored white. Protein domains of Dra-RNase J are shown in distinct colors and labeled. The 6 nt RNA is colored orange. Zn^{2+} and Mn^{2+} are shown as magenta and cyan spheres, respectively. The relative domain movement is shown by the arrowheads. (**B**) Superimpositions of the dimer form of Dra-RNase J (wheat), Tth-RNase J/RNA (white) and Tth-RNase J apo (green, PDB code: 3BK1) structures. Two protomers (A and B) are labeled respectively. (**C**) The active site of RNaseJ-UMP. Residues involved in metal chelation are shown as sticks. Zn^{2+} coordination is indicated by black dashed lines. The bridging water is shown as red sphere. (**D**) Nuclease assays of mutant Dra-RNase J proteins (alanine substitutions) from (C), using the same RNA and reaction condition (5 mM Mn^{2+}) as in Figure 1B.

main (residues 478–559; Figure 2A). The overall and catalytic core (the β-lactamase and β-CASP domain) of Dra-RNase J could be superimposed on the Tth-RNase J/RNA complex (PDB code: 3T3N) with an rmsd value of 0.978 and 0.931 Å over Cα atoms, respectively. Compared with the Tth-RNase J/RNA complex, the β-CASP domain of Dra-RNase J is oriented further away from the β-lactamase domain, resulting in a much more open cleft capable of accommodating the substrate RNA (Figure 2A). The angle between these two domains (measured between the Cα of residues Asp61, Thr219 and Glu269) increases by ∼7 degree, which creates a wider channel for RNA binding (Figure 2A and B). On the other hand, the linker α-helix (α13) and C-terminal domain of Dra-RNase J, especially α14 and α15, show noticeable movement (Figure 2A and B). Such conformational change is probably induced by the chelation of additional divalent cations at the dimer interface, which further tightens the dimerization of Dra-RNase J. Moreover, two loops (β22-α13 and β3-β4 loop) located within the β-lactamase domain also show noticeable deviations that facilitate the metal ion binding (Figure 2B and Supplementary Figure S4).

In RNaseJ-UMP, the catalytic center consists of two metal ions and two bridging ligands (Figure 2C and Supplementary Figure S3), a water molecule and the side chain carboxylate oxygen atom of Asp175 (motif IV). These two metal ions are bound in octahedral configuration by five histidines and two aspartate residues that one metal ion is coordinated by His84, His86 (motif II) and His153 (motif III), whereas Asp88, His89 (motif II) and His403 (motif V/C) are the ligands to the other one (Figure 2C). Such active site architecture is identical to that of RNase Z structure, a β-lactamase family nuclease involved in tRNA maturation (Supplementary Figure S5) (29,30). Ala substitutions of these conserved residues impair the Dra-RNase J nuclease activity to various degrees, but only the D175A completely abolishes the nuclease activity (Figure 2D). The D175A mutant protein was therefore used for RNaseJ-

RNA co-crystallization. To confirm the presence of Zn^{2+} in the catalytic center, RNaseJ-UMP crystals were grown under Mg^{2+} condition and checked by X-ray fluorescence analysis at synchrotron, which gave a strong peak at the Zn K-Edge (data not shown). The position of the Zn^{2+} ions was also verified based on the anomalous scattering data, which confirmed that both metal ions in the active site are Zn^{2+}. These results are consistent with the earlier biochemical observations that Dra-RNase J prefers Zn^{2+} for catalysis (Figure 1B).

RNA binding and catalysis

We solved the crystal structure of catalytic inactive mutant (D175A) Dra-RNase J complexed with synthesized 6 nt 5′-monophosphate RNA molecule (pUUUUUU). The electron density at 1.7 Å resolution clearly shows the RNA bound in a conformation that is ready to undergo cleavage (Figure 3A and Supplementary Figure S6). The active site is well formed with the RNA scissile phosphate centered on two properly coordinated Zn^{2+} ions (Figure 3A and B). Compared with the RNaseJ-UMP structure, the distance between these two Zn^{2+} ions increases by ∼0.2 Å, which is possibly due to the lack of one of the bridging ligands Asp175 (Figure 3B). Interactions between Dra-RNase J and substrate RNA phosphate groups are mainly mediated by a number of Arg, Ser, Thr and Tyr residues (Figure 3A and Supplementary Figure S7). In contrast, limited contacts with the first three bases have been detected, which facilitate catalysis (Figure 3A). Dra-RNase J could also act on DNA but clearly prefers RNA *in vitro* (Supplementary Figure S8). Indeed, Gln316 is the only residue that is hydrogen bonded to the 2′ oxygen, which may be responsible for discrimination between substrate RNA and DNA (Supplementary Figure S9). It is worth noting that there is no direct protein–RNA interaction beyond the 5th nt of the substrate RNA, which may explain the weak electron density of the last nucleotide (Figure 3A). A conserved 5′-monophosphate binding pocket was observed in RNaseJ-RNA structure. The loop (β17-α11) connecting the β-lactamase and β-CASP domain interacts with the phosphate moiety through hydrogen bonds, van der Waals's interactions, and indirect contacts through waters (Figure 3B and Supplementary Figure S10). Ala substitutions of both His377 and S379 dramatically reduced the nuclease activity, which is coherent with the 5′ -monophosphate ends preference of Dra-RNase J (Figure 3C).

Close inspection of the RNaseJ-RNA electron density map (Fo-Fc omit map for RNA) revealed an additional sphere electron density in the active site (Supplementary Figure S6). At 1.7 Å resolution, it is interpreted as a hydroxide ion, which is bound to two catalytic Zn^{2+} ions as a bridging ligand (Figure 3B). Such hydroxide ion has also been observed in the structure of CPSF-73, the representative member of the β-CASP nucleases, and proposed to be the nucleophile to cleave a scissile phosphodiester bond (31). Indeed, in RNaseJ-RNA, the hydroxide ion is located directly below the scissile phosphate at a distance of 3.4 Å (Figure 3B). For the RNA cleavage reaction, which generates 5′ phosphate and 3′ OH, it requires a nucleophile to be on the 5′ side poised for the in-line attack. However, the angle between the hydroxide ion, scissile phosphate and O3′ leaving group is ∼140 degree, which explains the inactivation of the D175A mutant protein. The conserved residue His381 (motif B), which is located opposite the direction of nucleophilic attack, is hydrogen bonded to Asp209 (motif A) and the oxygen atom of the scissile phosphate group (Figure 3B). Ala substitution of H381 dramatically impaired the enzymatic activity (Figure 3C), suggesting that this residue is most likely involved in the product stabilization. Configured around the scissile phosphate group, the active site is arguably the most reaction ready among the β-CASP nucleases crystallized so far. In summary, RNase J, as well as other β-lactamase family proteins such as RNase Z, uses the two-metal-ion catalysis (Figure 3D) as used by many nucleic acid processing enzymes (32–34). Following deprotonation of a water molecule by an aspartic acid general base (Asp88 in Dra-RNase J), the resultant divalent metal ion-bridging hydroxyl attacks the scissile phosphodiester bond. After bond breakage, His381 acts as a general acid to protonate the leaving group to stabilize the reaction products (Figure 3D).

The critical role of divalent cations in Dra-RNase J dimerization

Divalent cations, either Mn^{2+} or Mg^{2+} ions, were required for Dra-RNase J crystal growth. Crystals initially obtained in the presence of Mg^{2+} ions only diffracted to ∼2.6 Å. Despite that the catalytic core of Dra-RNase J was interpretable, the electron density of the C-terminal portion following the linker α-helix (α13) was weak and could not be modeled (Supplementary Figure S11). The entire Dra-RNase J structure was finally solved using crystals grown in the presence of Mn^{2+}, which dramatically improved the electron density map of the C-terminal domain as well as the diffraction quality (Supplementary Figure S11). A strong positive difference density peak close to the linker α-helix was observed in both copies of Dra-RNase J in the crystallographic asymmetric unit of both the RNaseJ-UMP and RNaseJ-RNA (Figure 4A and Supplementary Figure S12) structures, which is interpreted as the Mn^{2+} present at 100 mM in the crystallization buffers. Three conserved residues, two main chain carbonyl oxygen, and one water molecule coordinate this Mn^{2+}. Three of them (Gly59, Asp61 and Asp456) are from one protomer and the rest (Gln476 and Glu477) are from the other one (Figure 4A). Ala substitution of these residues dramatically decreased the exonuclease activity, suggesting that this metal ion-mediated dimerization is important for the cleavage (Figure 4B).

As mentioned earlier, Dra-RNase J forms a dimer in the crystallographic asymmetric unit. Compared with Tth-RNase J, which has no additional metal ion present at the dimer interface, two metal-binding loops (α15-β25 and β22-α13 loop) in Dra-RNase J are shifted toward each other to further tighten the protein dimer (Figure 4A). Indeed, in the presence of 10 mM EDTA, Dra-RNase J itself exists in a dynamic equilibrium between monomer (∼61.6 kDa) and homodimer (∼123.3 kDa) states, as shown by size exclusion chromatography (Superdex 200 10/300 GL column; Figure 4C). While the elution profile shifts toward

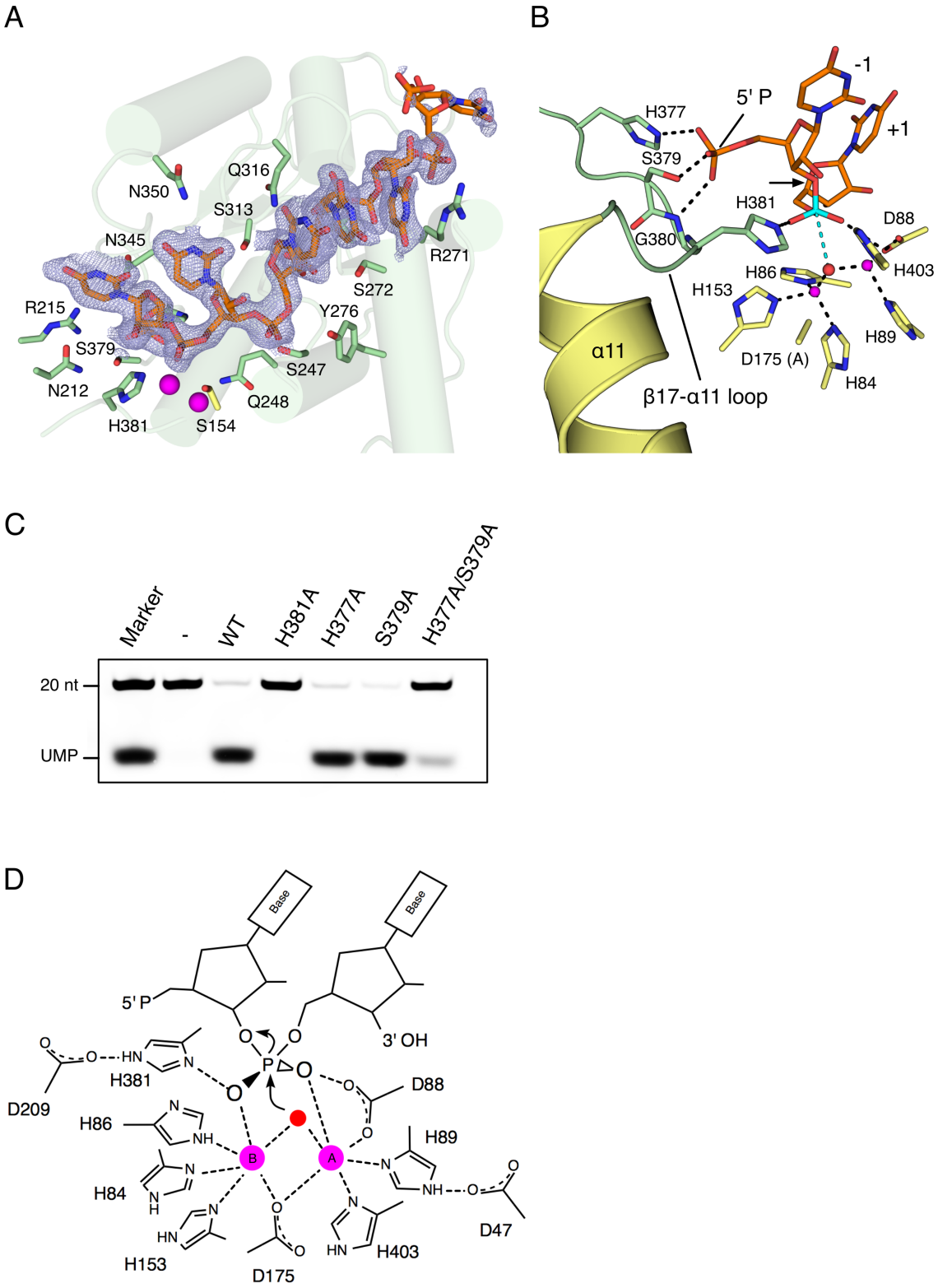

Figure 3. RNA recognition and catalysis. (**A**) The protein–RNA interaction. Protein side chains are shown as sticks. The electron density of 6 nt RNA is shown in blue with the refined $2F_o$-F_c map contoured at 1σ. (**B**) The catalytic center and 5′-monophosphate moiety recognition. The bridging hydroxide ion is shown as red sphere. The hydroxide ion is 3.4 Å from the scissile phosphate (cyan) as indicated by the cyan dashed line. The black arrowhead indicates the position of P-O bond breakage. First two nucleotides are shown and labeled as −1 and +1 according to their relative position to the scissile phosphate. (**C**) Nuclease assays of mutant Dra-RNase J proteins (alanine substitutions of residues located at loop β17-α11), using the same RNA and reaction condition (5 mM Mn^{2+}) as in Figure 1B. (**D**) A proposed mechanism for RNase J two-metal-ion catalysis. Two Zn^{2+} ions are highlighted in magenta, and the nucleophile hydroxide ion in red. The arrowheads show the direction of nucleophilic attack. Hydrogen bonds and metal-ion coordination are shown as dashed lines.

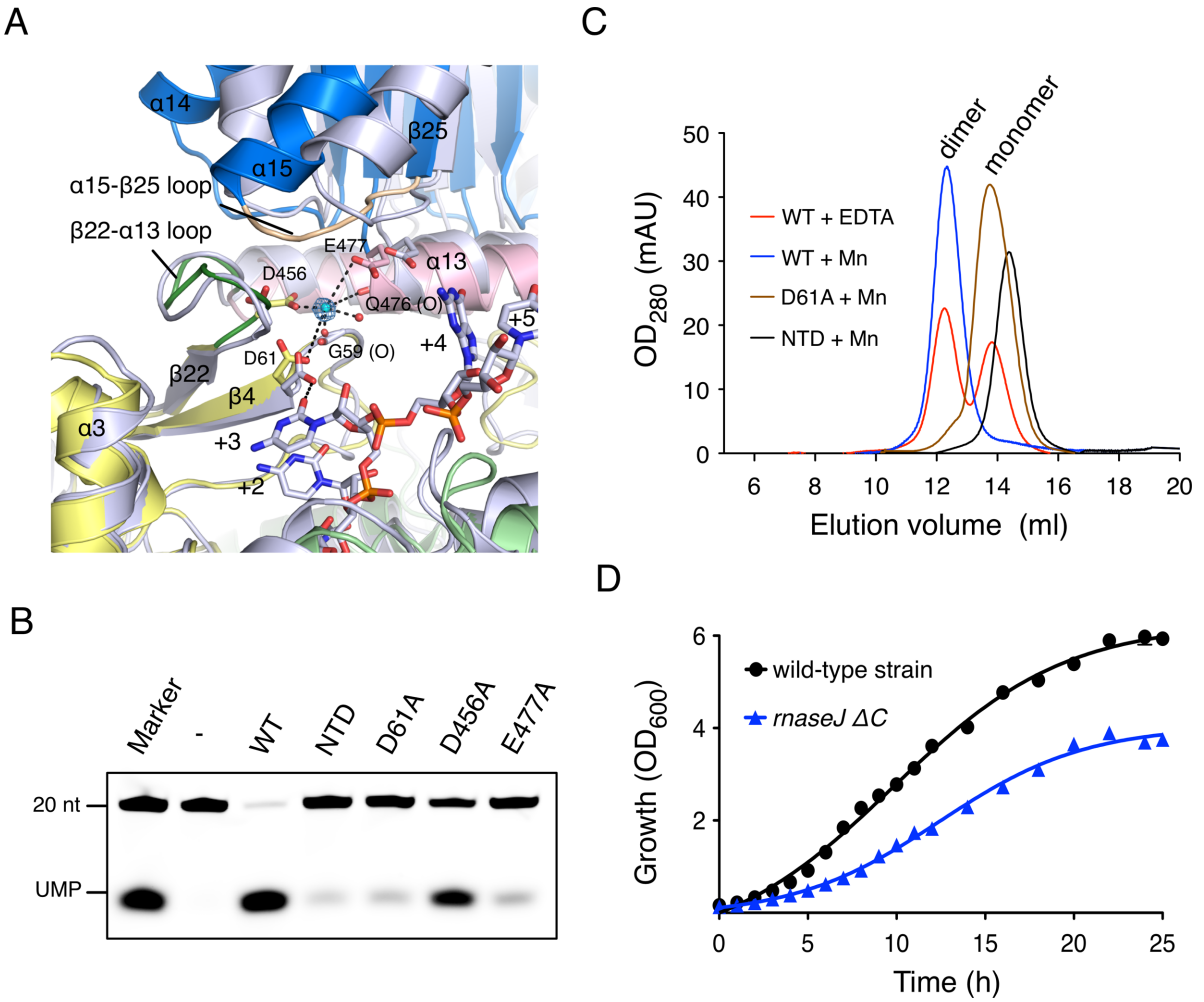

Figure 4. Critical role of Mn^{2+} at the dimer interface. (**A**) Mn^{2+} coordination at the dimer interface. RNaseJ-RNA is superimposed on the Tth-RNase J (PDB code: 3T3N) complexed with RNA (same coloring as in Figure 2A). The refined electron density map (2Fo-Fc) contoured at 5σ is superimposed on the Mn^{2+}. Two shifted loops are shown in green and wheat, respectively. The nucleotides of Tth-RNase J/RNA are labeled as +2, +3, +4 and +5 according to the relative position to the scissile phosphate. (**B**) Nuclease assays of mutant (D61A, D456A and E477A) or truncated (NTD, residues 1–450) Dra-RNase J proteins, using the same RNA and reaction condition (5 mM Mn^{2+}) as in Figure 1B. (**C**) Size exclusion chromatography of wild type, mutant (D61A) and truncated (NTD) Dra-RNase J proteins incubated with EDTA or Mn^{2+} on Superdex 200 10/300 GL column. The peaks correspond to monomeric or dimeric Dra-RNase J are labeled and colored differently. (**D**) Growth curves of wild type (black line) and heterozygous C-terminal truncated *rnaseJ* mutant strain (*rnaseJ ΔC*, blue line).

the dimer when additional 10 mM Mn^{2+} is present in the buffer, Ala substitution of Asp61 shifts the equilibrium position toward the monomer (Figure 4C). Thus, the binding of divalent cations at the dimerization interface facilitates dimerization of Dra-RNase J. It is noteworthy that the Asp52 of Tth-RNase J (equivalent to Asp61 in Dra-RNase J) interacts with the base of the +3 nucleotide (the position relative to the scissile phosphate; Figure 4A), suggesting that this conserved residue is probably involved in both protein dimerization and RNA translocation. We tested whether mutation of D61 had a preferential impact on either the exo- or endonucleolytic activity of Dra-RNase J. Indeed, D61A mutant Dra-RNase J protein exhibited relatively strong endonuclease activity on double hairpin RNA *in vitro* (Supplementary Figure S13), which has cleavage site similar to *B. subtilis* RNase J1 (12). In contrast, the wild type Dra-RNase J showed little endonuclease activity, indicating that the switch of RNase J exo/endonuclease activities is possibly regulated by the protein dimerization state. The catalytic core of Dra-RNase J (NTD, residues 1–450) was expressed and purified to further confirm the role of the divalent-cation enhanced dimerization. Dra-Rnase J lacking the C-terminal domain exhibited impaired exonuclease but enhanced endonuclease activity (Figure 4B and Supplementary Figure S13) and could no longer form a homodimer (Figure 4C). Unsurprisingly, complete inactivation of the Dra-RNase J C-terminal domain is lethal. The heterozygous mutant containing about 20% residual full-length *rnaseJ* genes (data not shown) grew noticeably slower than the wild-type strain (Figure 4D), indicating that the Dra-RNase J dimerization plays a vital role *in vivo*.

As discussed above, Mn^{2+} appeared to be the most effective divalent cation for Dra-RNase J catalysis. This metal preference might be due to the following: firstly, compared

with Mg^{2+}, Mn^{2+} has a similar ionic radius but less rigid coordination requirements (35,36). Moreover, Mn^{2+} is able to bind to the carbonyl oxygen of the main chain (37), making it suitable for the metal-chelation in the dimerization interface; secondly, recent studies revealed a correlation between the bacterial ionizing radiation resistance and the intracellular Mn/Fe ratio (38). The unusual accumulation of Mn^{2+} ions in *D. radiodurans*, the most known radioresistant organisms, plays a critical role in reactive oxygen species scavenging and protein protection (39). In addition, growing evidence suggests that the Mn^{2+} serves as a universal modulator of the enzymes involved in DNA repair in *D. radiodurans* (27,40). Thus, the Mn^{2+} preference of Dra-RNase J might also be an example of the evolutionary adaptation.

CONCLUDING REMARKS

RNase J is a key ribonuclease involved in RNA processing in Gram-positive bacteria. The biochemical and structural studies presented in this study suggest that RNase J is a zinc-dependent nuclease using two-metal-ion catalysis. The loop region linking the β-lactamase and β-CASP domain is involved in both 5′-monophosphate moiety recognition and product stabilization. Divalent cations play a critical role in RNase J dimerization, which further stimulates the exonuclease activity. The switch between exo- and endonucleolytic activity of RNase J could be possibly regulated by the protein dimerization. Also, our findings of the Mn^{2+} preference of Dra-RNase J provides the first evidence that the high intracellular Mn^{2+} concentration in *D. radiodurans* cells may serve to modulate the activity of enzymes involved in RNA metabolism.

ACCESSION NUMBERS

The coordinates and structural factors of Dra-RNase J complexed with RNA or UMP have been deposited into the Protein Data Bank under the accession code 4XWW (RNase J_d-RNA) and 4XWT (RNase J-UMP).

SUPPLEMENTARY DATA

Supplementary Data are available at NAR Online.

ACKNOWLEDGEMENT

We would like to thank the staff at the Shanghai Synchrotron Radiation Facility (SSRF in China) for assistance in data collection. We also thank Dr. David Waugh (National Cancer Institute) for the generous gift of the protein expression vector pET28a-MBP-TEV.

FUNDING

National Basic Research Program of China [2015CB910600]; National Natural Science Foundation of China [31210103904, 31370102]; Ministry of Agriculture of China [2014ZX08009003–002]; Agro-scientific Research in the Public Interest from the Ministry of Agriculture of China [201103007]; Natural Science Foundation and Educational Commission of Zhejiang province [LY13C010001, Y201329892]; Fundamental Research Funds for the Central Universities from Zhejiang University and the Key Innovation Team Program of Zhejiang Province [2010R50033]. Funding for open access charge: National Basic Research Program of China [2015CB910600]; National Natural Science Foundation of China [31210103904, 31370102]; Ministry of Agriculture of China [2014ZX08009003–002]; Agro-scientific Research in the Public Interest from the Ministry of Agriculture of China [201103007]; Natural Science Foundation and Educational Commission of Zhejiang province [LY13C010001, Y201329892]; Fundamental Research Funds for the Central Universities from Zhejiang University and the Key Innovation Team Program of Zhejiang Province [2010R50033].
Conflict of interest statement. None declared.

REFERENCES

1. Bandyra,K.J., Bouvier,M., Carpousis,A.J. and Luisi,B.F. (2013) The social fabric of the RNA degradosome. *Biochim. Biophys. Acta*, **1829**, 514–522.
2. Gorna,M.W., Carpousis,A.J. and Luisi,B.F. (2012) From conformational chaos to robust regulation: the structure and function of the multi-enzyme RNA degradosome. *Q. Rev. Biophys.*, **45**, 105–145.
3. Condon,C. (2003) RNA processing and degradation in Bacillus subtilis. *Microbiol. Mol. Biol. Rev.*, **67**, 157–174.
4. Carpousis,A.J., Luisi,B.F. and McDowall,K.J. (2009) Endonucleolytic initiation of mRNA decay in Escherichia coli. *Prog. Mol. Biol. Transl. Sci.*, **85**, 91–135.
5. Mackie,G.A. (2013) RNase E: at the interface of bacterial RNA processing and decay. *Nat. Rev. Microbiol.*, **11**, 45–57.
6. Jain,C., Deana,A. and Belasco,J.G. (2002) Consequences of RNase E scarcity in Escherichia coli. *Mol. Microbiol.*, **43**, 1053–1064.
7. Redko,Y., Aubert,S., Stachowicz,A., Lenormand,P., Namane,A., Darfeuille,F., Thibonnier,M. and De Reuse,H. (2013) A minimal bacterial RNase J-based degradosome is associated with translating ribosomes. *Nucleic Acids Res.*, **41**, 288–301.
8. Taverniti,V., Forti,F., Ghisotti,D. and Putzer,H. (2011) Mycobacterium smegmatis RNase J is a 5′-3′ exo-/endoribonuclease and both RNase J and RNase E are involved in ribosomal RNA maturation. *Mol. Microbiol.*, **82**, 1260–1276.
9. Madhugiri,R. and Evguenieva-Hackenberg,E. (2009) RNase J is involved in the 5′-end maturation of 16S rRNA and 23S rRNA in Sinorhizobium meliloti. *FEBS Lett.*, **583**, 2339–2342.
10. Mathy,N., Benard,L., Pellegrini,O., Daou,R., Wen,T. and Condon,C. (2007) 5′-to-3′ exoribonuclease activity in bacteria: role of RNase J1 in rRNA maturation and 5′ stability of mRNA. *Cell*, **129**, 681–692.
11. Condon,C., Putzer,H., Luo,D. and Grunberg-Manago,M. (1997) Processing of the Bacillus subtilis thrS leader mRNA is RNase E-dependent in Escherichia coli. *J. Mol. Biol.*, **268**, 235–242.
12. Even,S., Pellegrini,O., Zig,L., Labas,V., Vinh,J., Brechemmier-Baey,D. and Putzer,H. (2005) Ribonucleases J1 and J2: two novel endoribonucleases in B.subtilis with functional homology to E.coli RNase E. *Nucleic Acids Res.*, **33**, 2141–2152.
13. Durand,S., Gilet,L., Bessieres,P., Nicolas,P. and Condon,C. (2012) Three essential ribonucleases-RNase Y, J1, and III-control the abundance of a majority of Bacillus subtilis mRNAs. *PLoS Genet.*, **8**, e1002520.
14. Bechhofer,D.H. (2011) Bacillus subtilis mRNA decay: new parts in the toolkit. *Wiley Interdiscip. Rev. RNA*, **2**, 387–394.
15. Britton,R.A., Wen,T., Schaefer,L., Pellegrini,O., Uicker,W.C., Mathy,N., Tobin,C., Daou,R., Szyk,J. and Condon,C. (2007) Maturation of the 5′ end of Bacillus subtilis 16S rRNA by the essential ribonuclease YkqC/RNase J1. *Mol. Microbiol.*, **63**, 127–138.
16. Mathy,N., Hebert,A., Mervelet,P., Benard,L., Dorleans,A., Li de la Sierra-Gallay,I., Noirot,P., Putzer,H. and Condon,C. (2010) Bacillus

subtilis ribonucleases J1 and J2 form a complex with altered enzyme behaviour. *Mol. Microbiol.*, **75**, 489–498.
17. Yao,S., Sharp,J.S. and Bechhofer,D.H. (2009) Bacillus subtilis RNase J1 endonuclease and 5′ exonuclease activities in the turnover of DeltaermC mRNA. *RNA*, **15**, 2331–2339.
18. Mader,U., Zig,L., Kretschmer,J., Homuth,G. and Putzer,H. (2008) mRNA processing by RNases J1 and J2 affects Bacillus subtilis gene expression on a global scale. *Mol. Microbiol.*, **70**, 183–196.
19. Newman,J.A., Hewitt,L., Rodrigues,C., Solovyova,A., Harwood,C.R. and Lewis,R.J. (2011) Unusual, dual endo- and exonuclease activity in the degradosome explained by crystal structure analysis of RNase J1. *Structure*, **19**, 1241–1251.
20. Dorleans,A., Li de la Sierra-Gallay,I., Piton,J., Zig,L., Gilet,L., Putzer,H. and Condon,C. (2011) Molecular basis for the recognition and cleavage of RNA by the bifunctional 5′-3′ exo/endoribonuclease RNase J. *Structure*, **19**, 1252–1261.
21. Li de la Sierra-Gallay,I., Zig,L., Jamalli,A. and Putzer,H. (2008) Structural insights into the dual activity of RNase J. *Nature Struct. Mol. Biol.*, **15**, 206–212.
22. Zhang,H., Xu,Q., Lu,M., Xu,X., Wang,Y., Wang,L., Zhao,Y. and Hua,Y. (2014) Structural and functional studies of MutS2 from Deinococcus radiodurans. *DNA Repair*, **21**, 111–119.
23. Kabsch,W. (2010) Xds. *Acta Crystallogr. D Biol. Crystallogr.*, **66**, 125–132.
24. McCoy,A.J., Grosse-Kunstleve,R.W., Adams,P.D., Winn,M.D., Storoni,L.C. and Read,R.J. (2007) Phaser crystallographic software. *J. Appl. Crystallogr.*, **40**, 658–674.
25. Adams,P.D., Afonine,P.V., Bunkoczi,G., Chen,V.B., Davis,I.W., Echols,N., Headd,J.J., Hung,L.W., Kapral,G.J., Grosse-Kunstleve,R.W. *et al.* (2010) PHENIX: a comprehensive Python-based system for macromolecular structure solution. *Acta Crystallogr. D Biol. Crystallogr.*, **66**, 213–221.
26. Emsley,P., Lohkamp,B., Scott,W.G. and Cowtan,K. (2010) Features and development of Coot. *Acta Crystallogr. D Biol. Crystallogr.*, **66**, 486–501.
27. Jiao,J., Wang,L., Xia,W., Li,M., Sun,H., Xu,G., Tian,B. and Hua,Y. (2012) Function and biochemical characterization of RecJ in Deinococcus radiodurans. *DNA Repair*, **11**, 349–356.
28. Kolev,N.G., Yario,T.A., Benson,E. and Steitz,J.A. (2008) Conserved motifs in both CPSF73 and CPSF100 are required to assemble the active endonuclease for histone mRNA 3′-end maturation. *EMBO Rep.*, **9**, 1013–1018.
29. Redko,Y., Li de la Sierra-Gallay,I. and Condon,C. (2007) When all's zed and done: the structure and function of RNase Z in prokaryotes. *Nat. Rev. Microbiol.*, **5**, 278–286.
30. Li de la Sierra-Gallay,I., Pellegrini,O. and Condon,C. (2005) Structural basis for substrate binding, cleavage and allostery in the tRNA maturase RNase Z. *Nature*, **433**, 657–661.
31. Mandel,C.R., Kaneko,S., Zhang,H., Gebauer,D., Vethantham,V., Manley,J.L. and Tong,L. (2006) Polyadenylation factor CPSF-73 is the pre-mRNA 3′-end-processing endonuclease. *Nature*, **444**, 953–956.
32. Zhao,Y., Gregory,M.T., Biertumpfel,C., Hua,Y.J., Hanaoka,F. and Yang,W. (2013) Mechanism of somatic hypermutation at the WA motif by human DNA polymerase eta. *Proc. Natl. Acad. Sci. U.S.A.*, **110**, 8146–8151.
33. Nakamura,T., Zhao,Y., Yamagata,Y., Hua,Y.J. and Yang,W. (2012) Watching DNA polymerase eta make a phosphodiester bond. *Nature*, **487**, 196–201.
34. Yang,W., Lee,J.Y. and Nowotny,M. (2006) Making and breaking nucleic acids: two-Mg2+-ion catalysis and substrate specificity. *Mol. Cell*, **22**, 5–13.
35. Maguire,M.E. and Cowan,J.A. (2002) Magnesium chemistry and biochemistry. *Biometals*, **15**, 203–210.
36. Harding,M.M. (2000) The geometry of metal-ligand interactions relevant to proteins. II. Angles at the metal atom, additional weak metal-donor interactions. *Acta Crystallogr. D Biol. Crystallogr.*, **56**, 857–867.
37. Bock,C.W., Katz,A.K., Markham,G.D. and Glusker,J.P. (1999) Manganese as a replacement for magnesium and zinc: Functional comparison of the divalent ions. *J. Am. Chem. Soc.*, **121**, 7360–7372.
38. Daly,M.J., Gaidamakova,E.K., Matrosova,V.Y., Vasilenko,A., Zhai,M., Venkateswaran,A., Hess,M., Omelchenko,M.V., Kostandarithes,H.M., Makarova,K.S. *et al.* (2004) Accumulation of Mn(II) in Deinococcus radiodurans facilitates gamma-radiation resistance. *Science*, **306**, 1025–1028.
39. Daly,M.J., Gaidamakova,E.K., Matrosova,V.Y., Vasilenko,A., Zhai,M., Leapman,R.D., Lai,B., Ravel,B., Li,S.M., Kemner,K.M. *et al.* (2007) Protein oxidation implicated as the primary determinant of bacterial radioresistance. *PLoS Biol.*, **5**, e92.
40. Heinz,K. and Marx,A. (2007) Lesion bypass activity of DNA polymerase A from the extremely radioresistant organism Deinococcus radiodurans. *J. Biol. Chem.*, **282**, 10908–10914.